Automated Autofluorescence Background Subtraction Algorithm for Biomedical Raman Spectroscopy

JIANHUA ZHAO, HARVEY LUI, DAVID I. McLEAN, and HAISHAN ZENG*

The Laboratory for Advanced Medical Photonics (LAMP), Department of Dermatology and Skin Science, University of British Columbia and Vancouver Coastal Health Research Institute and Cancer Imaging Department, BC Cancer Research Center, Vancouver, BC, Canada

A significant advantage of Raman spectroscopy as a noninvasive optical technique is its ability to detect subtle molecular or biochemical signatures within tissue. One of the major challenges for biomedical Raman spectroscopy is the removal of intrinsic autofluorescence background signals, which are usually a few orders of magnitude stronger than those arising from Raman scattering. A number of methods have been proposed for fluorescence background removal including excitation wavelength shifting, Fourier transformation, time gating, and simple or modified polynomial fitting. The single polynomial and the modified multi-polynomial fitting methods are relatively simple and effective, and thus are widely used in biological applications. However, their performance in real-time *in vivo* applications and low signal-to-noise ratio environments is sub-optimal. An improved automated algorithm for fluorescence removal has been developed based on modified multi-polynomial fitting, but with the addition of (1) a peak-removal procedure during the first iteration, and (2) a statistical method to account for signal noise effects. Experimental results demonstrate that this approach improves the automated rejection of the fluorescence background during real-time Raman spectroscopy and for *in vivo* measurements characterized by low signal-to-noise ratios.

Index Headings: **Raman spectroscopy; Fluorescence background removal; Biomedical Raman; Polynomial fitting.**

INTRODUCTION

As a noninvasive optical technique, Raman spectroscopy has been extensively used in investigations of biological tissues in recent years.[1–8] One major advantage of Raman spectroscopy is that it can detect subtle molecular or biochemical changes in tissue. Recent hardware system developments have substantially decreased spectral acquisition times, paving the way for Raman applications in clinical settings.[7,8]

The probability of Raman scattering is exceedingly low, being a few orders of magnitude less than the intrinsic fluorescence emission of biological tissues. Separating this concomitant autofluorescence from the Raman scattering signal in the acquired raw spectra is a significant challenge, particularly considering the complex spectral features associated with Raman scattering. Two basic approaches have been adopted for rejecting fluorescence in order to derive the true Raman signals:[9,10] instrumental and computational. Instrumental methods include shifted excitation[11,12] and time gating,[13] which requires hardware modification in the spectroscopic systems, whereas computational methods, facilitated by software, involve polynomial fitting,[1–8] Fourier transformation,[9,14,15] and spectral shifting.[15] The choice of fluorescence baseline removal is application dependent and ranges from being relatively simple for determining qualitative features to complicated hardware and software implementations for detailed quantitative analysis. A well-written article by Schulze et al. reviewed the selection of appropriate Raman baseline removal methods for automated applications.[9]

Shifted excitation is a promising method for suppressing fluorescence backgrounds, but it involves both hardware modifications and additional spectral processing.[16,17] Fourier transform filtering is one of the most accurate methods for fluorescence rejection, but it depends on direct human intervention to manually specify the upper and lower limits in the frequency domain. Not only is this time consuming, but the limits also differ from case to case.[14,15] Thus, for biomedical applications, the most popular fluorescence removal technique has proven to be polynomial fitting because of its simplicity and convenience.[2] Fluorescence can be mathematically modeled as a polynomial function, the order of which is selected to effectively remove the fluorescence baseline signal while at the same time minimizing the subtraction of the desired Raman scattering.[2] Based on empirical experience, fourth- to sixth-order polynomials provide the best fluorescence approximations for *in vivo* biomedical applications,[2,4,18–20] except for heavily pigmented lesions, for which a second-order polynomial is suggested.[6]

Raman spectra have been used for quantifying bio-molecules.[21–28] However, they are prone to variability or errors due to the somewhat arbitrary approach to choosing orders and fitting ranges. Recently, Lieber and Mahadevan-Jansen proposed a modified multi-polynomial fitting method that substantially improved the fluorescence background removal in Raman spectra processing.[10] In using this modified multi-polynomial method we have found that it is still subject to limitations, especially in real-time Raman processing systems and under high noise circumstances. In this paper, we present a method to further improve the modified multi-polynomial fitting method for fluorescence background removal. Experimental results show that this method can be fully automated and processed during real-time Raman spectroscopy.

FLUORESCENCE SUBTRACTION ALGORITHM

Polynomial Fitting (PolyFit) and Modified Multi-Polynomial Fitting (ModPoly). The primary advantage of polynomial fitting is its simplicity and effectiveness. It is faster than other methods and has been widely used for *in vivo* biomedical Raman applications. The weakness of polynomial fitting is its dependence on the spectral fitting range and the chosen polynomial order. As an example, Fig. 1a shows the raw spectroscopic signal from normal extensor forearm skin and the fitted polynomial fluorescence background under different conditions. The fitting results clearly differ according to polynomial order for the same spectral range (e.g., fifth- versus sixth-order polynomial for the 500–1800 cm^{-1} range) and also for different data ranges using the same polynomial

Received 7 May 2007; accepted 7 August 2007.
* Author to whom correspondence should be sent. E-mail: hzeng@bccrc.ca.

0003-7028/07/6111-1225$2.00/0

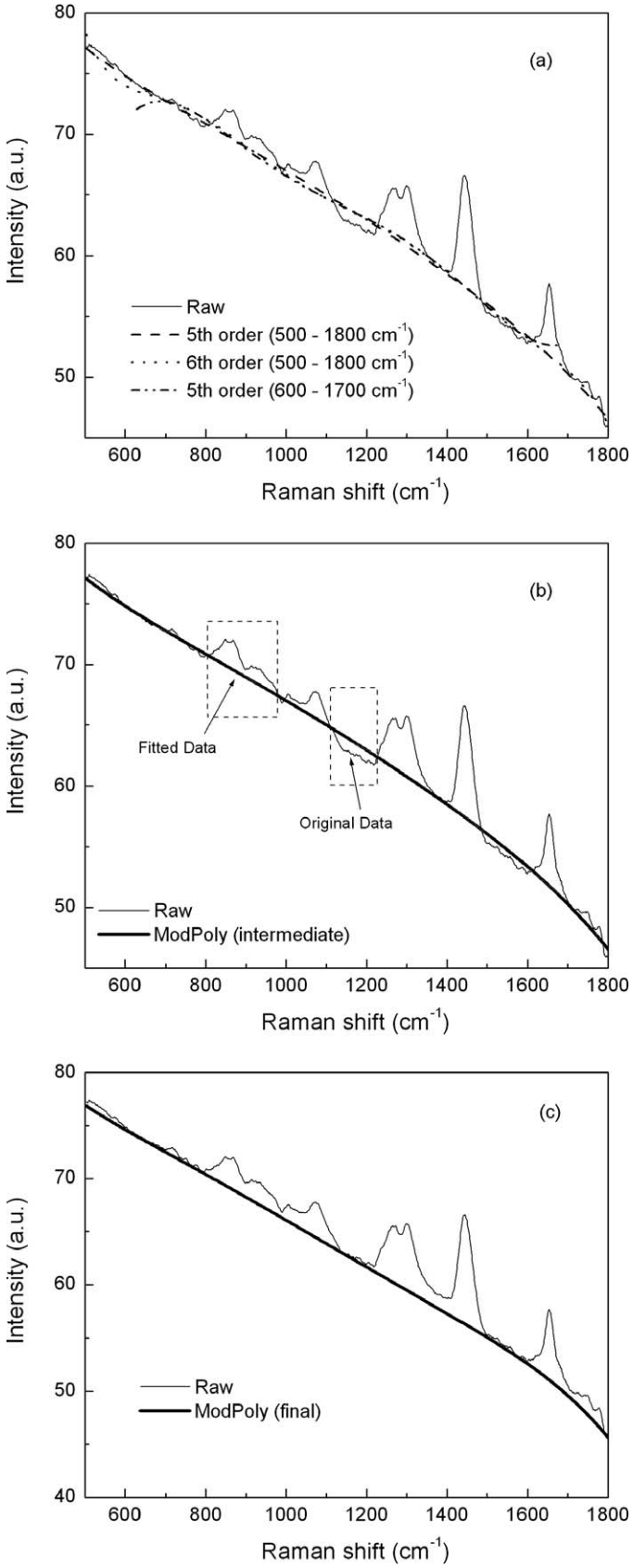

FIG. 1. (**a**) Raw Raman spectra from normal human extensor forearm skin under different polynomial fitting conditions: single polynomial fitting with fifth- and sixth-order polynomials for the data range between 500 cm^{-1} and 1800 cm^{-1}, and fifth-order polynomial fitting for the data range between 600 and 1700 cm^{-1}; (**b**) an intermediate fitting using the modified multi-polynomial fitting method, demonstrating the data segments to be concatenated for the next round of polynomial fitting; (**c**) the final fluorescence background fitted using the modified polynomial fitting method.

order (e.g., fifth-order polynomial for 500–1800 cm^{-1} versus 600–1700 cm^{-1}). Thus, errors may ensue if these differences are not carefully considered or compensated for, especially in quantitative analysis. In order to reduce the limitations of single polynomial fitting for fluorescence background removal, Lieber and Mahadevan-Jansen proposed a modified multi-polynomial fitting (ModPoly) method.[10] This is an iterative polynomial algorithm in which the spectral ordinate values for the raw spectrum are compared to the polynomial model at each wavenumber. For each successive round of polynomial fitting the lower values for each wavenumber are selected and then concatenated to construct a modified spectrum, which is then in turn re-fitted. An example of an intermediate step during the ModPoly fitting is shown in Fig. 1b. The right-hand box shows where the original signal is lower than the fitted function and therefore the original data are used, while the left-hand box shows where the original data are greater than the fitted function and thus the fitted data is incorporated into the input for the next round of polynomial fitting. The result after the final iteration in the ModPoly fitting method is shown in Fig. 1c. In comparison with Fig. 1a, the ModPoly algorithm substantially improves fluorescence rejection in biomedical Raman measurements. However, there are still a number of limitations for automated fluorescence removal in the setting of real-time Raman applications: (1) the contribution of noise is not properly dealt with and this could have adverse effects, especially in high noise situations; in the ModPoly method, noise that is greater than the fitted function is incorrectly treated as Raman signal and is therefore replaced by the fitted function in the next round of polynomial fitting; (2) similar to single polynomial fitting, ModPoly can introduce artificial peaks where the original data in peak-free regions are slightly higher than the curvatures of the polynomial curve and thus are incorrectly replaced by the fitted ones; (3) the contribution of some major large peaks in the polynomial fitting is significant, which may bias the fitting results; and (4) it takes from 20 to 500 iterations to compute as compared to a single polynomial fitting, which could be fairly long for real-time spectroscopy.

Improved Modified Multi-Polynomial Fitting (I-ModPoly). For practical automated fluorescence rejection, subjective direct human intervention must be minimized, and thus the concerns with the ModPoly method must be addressed to obtain more truly representative Raman spectra. Our method for improving the above ModPoly fitting method takes into account signal noise distortion and the influence of large Raman peaks on fluorescence background fitting. It combines the addition of a peak removal procedure during the first iteration and takes into account the noise effect that is propagated with the ModPoly fitting method. The algorithm is denoted as I-ModPoly.

A detailed diagram of the I-ModPoly algorithm is shown in Fig. 2. It starts from a single polynomial fitting $P(\nu)$ using the raw Raman signal $O(\nu)$, where ν is the Raman shift in cm^{-1}. Then the residual $R(\nu)$ and its standard deviation, *DEV*, are calculated as follows:

$$R(\nu) = O(\nu) - P(\nu) \tag{1}$$

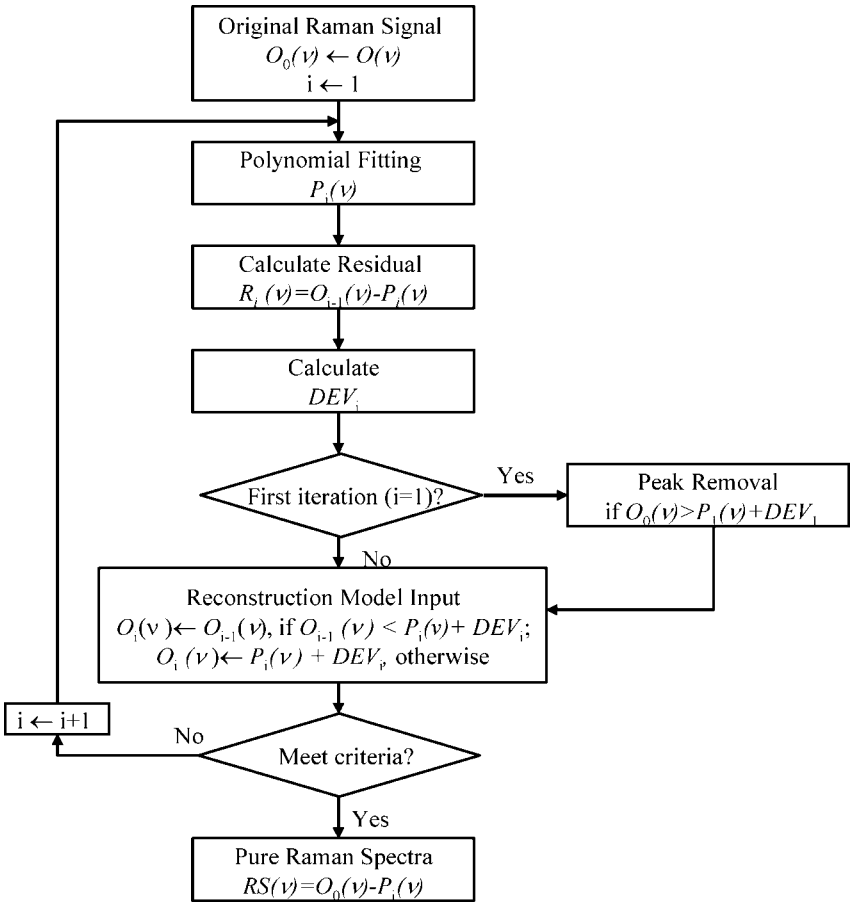

FIG. 2. Detailed diagram of our improved modified multi-polynomial fitting method (I-ModPoly).

$$DEV = \sqrt{\frac{\left(R(v_1)-\overline{R}\right)^2+\left(R(v_2)-\overline{R}\right)^2+\cdots+\left(R(v_n)-\overline{R}\right)^2}{n}} \quad (2)$$

with n representing the number of data points on the spectral curve, and

$$\overline{R} = \frac{R(v_1)+R(v_2)+\cdots+R(v_n)}{n} \quad (3)$$

The quantity *DEV* is considered an approximation of the noise level. Instead of comparing the original data with the fitted function as the standard for constructing the data for the next round of fitting input as in the ModPoly method, here we base the comparison on the sum of the fitting function plus the value of *DEV*, which we define as *SUM*. Values that are greater than *SUM* are regarded as Raman signal. The concatenated data in the Raman signal peak regions are constructed from the *SUM* for the next round of fitting rather than from the fitting function itself as in the ModPoly method. This provides a means for taking into account the noise effect and avoiding artificial peaks that may arise from the noise.

In order to minimize the distortion of the polynomial fitting by major Raman signals, the major peaks are identified during the first iteration of polynomial fitting. The data in the major peak regions are removed from the following rounds of fitting. Peak removal is limited to the first iteration only to prevent unnecessary data rejection. The iterative polynomial fitting procedure is stopped as judged by $|(DEV_i - DEV_{i-1})/DEV_i| < 5\%$, which indicates that further iterations cannot significantly improve the fitting. As in many iterative computation methods, this value can be empirically adjusted by the user according to the problem involved and computation time allowed. However, we suggest that once selected, this value should be fixed in the whole process for a given clinical study. The final polynomial fit is regarded as the fluorescence background. The final Raman spectra are derived from the raw spectra by subtracting the final polynomial fit function.

SIMULATION AND EXPERIMENTAL RESULTS AND DISCUSSIONS

Simulation Results and Discussions. In order to provide quantitative comparison between the three methods, a phantom Raman spectrum was mathematically generated as a series of Lorentzian peaks:

$$y_R = \sum_{i=1}^{N} \frac{2A_{0i}}{\pi} \frac{\omega_{0i}}{4(r-r_{0i})^2+\omega_{0i}^2} \quad (4)$$

where r_{0i} is the position of the peak, A_{0i} is the total area under the curve from the baseline, and ω_{0i} is the bandwidth of the peak at the full-width at half-maximum (FWHM). The parameters used in the simulation are listed in Table I. Twelve

TABLE I. The Lorentzian function parameters used for constructing the phantom "Raman spectrum".

r_0	ω_0	A_0
856	51	43
944	43	34
1002	8	16
1027	12	13
1071	30	42
1123	79	8
1259	24	60
1265	24	70
1302	20	62
1341	15	19
1444	17	105
1652	21	74

peaks were chosen to simulate the tissue Raman signal. The "fluorescence background" was generated using a fifth-order polynomial:

$$y_f = 3.822 - 9.06 \times 10^{-1} r + 1.560 \times 10^{-3} r^2 - 1.443 \times 10^{-6} r^3 + 6.721 \times 10^{-10} r^4 - 1.240 \times 10^{-13} r^5 \quad (5)$$

where y_f represents the "fluorescence" intensity, and r represents the "Raman shift". The coefficients were chosen arbitrarily but the shape was similar to the fluorescence background of *in vivo* tissue. The amplitude of random noise, generated by a random function, was equal to 3% of the maximum "Raman" peak intensity. The computer-generated spectrum with the above parameters is shown in Fig. 3a. Assuming the background of the phantom spectra was totally blind to us, a fourth-, fifth-, and sixth-order polynomial of the three methods were used to fit the "fluorescence background" of the generated spectrum. The fitted "Raman" spectrum is shown in Fig. 3b. The coefficients of determination R^2 for the (single PolyFit, ModPoly, and I-ModPoly) fitting methods are (0.80, 0.90, and 0.90) for the fourth-, (0.85, 0.98, and 0.99) for the fifth-, and (0.80, 0.98, and 0.99) for the sixth-order fitting, respectively. This demonstrates that a single polynomial fitting cannot fully recover the generated pure Raman spectra ($R^2 \leq 0.85$). ModPoly provides better ($R^2 \leq 0.98$) and I-ModPoly provides the best ($R^2 \leq 0.99$) fitting for recovering the pure original "Raman spectra". Both ModPoly and I-ModPoly are much less dependent on the polynomial orders than the single PolyFit, and the independence for I-ModPoly is slightly better than for ModPoly. I-ModPoly took 18 times less computing time than ModPoly for this example.

There are two aspects contributing to the decrease of computing time in I-ModPoly. One is that the dataset used in I-ModPoly fitting is much smaller than that of ModPoly fitting because the data points of the strong Raman peaks are removed in the I-ModPoly fitting. The other aspect is that there are less iterations in I-ModPoly fitting than ModPoly fitting, especially for a low signal-to-noise spectrum.

Experimental Results and Discussions. In order to demonstrate the utility of the proposed fluorescence removal algorithm, experiments were carried out to measure the Raman spectra of biological samples and human skin *in vivo* using a home-made rapid near-infrared (NIR) Raman system.[7] Briefly, the rapid Raman system consists of an external cavity

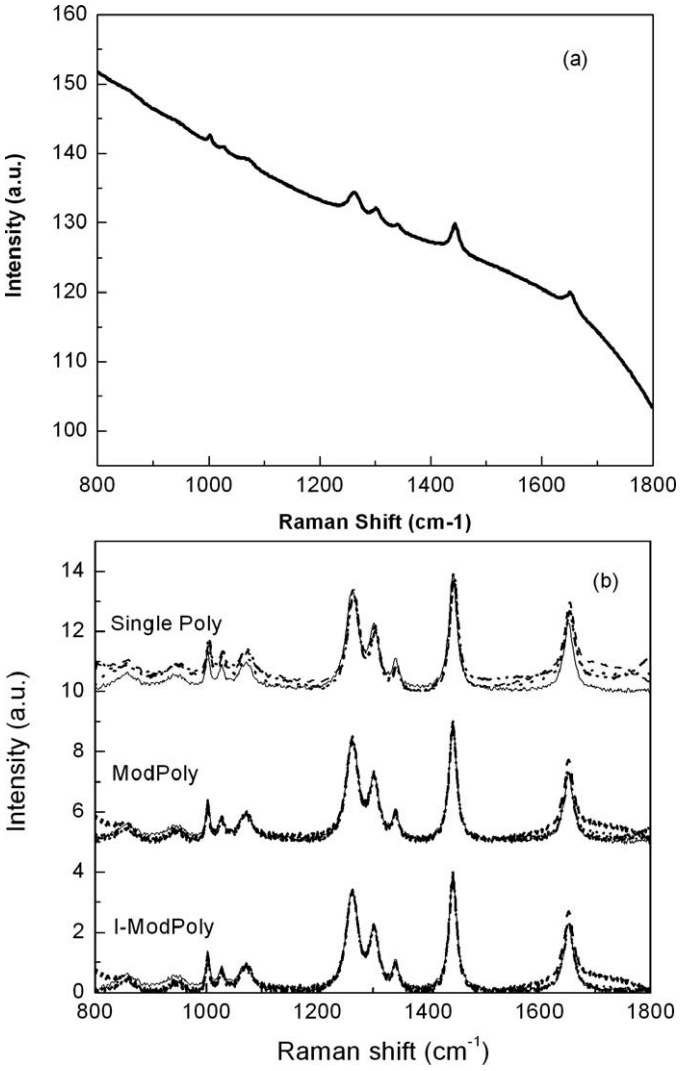

FIG. 3. (**a**) Mathematically generated "Raman spectrum" using 12 Lorentzian functions and a fifth-order polynomial function, and (**b**) the pure "Raman" spectra after fluorescence background removal using the three methods. The solid line, dashed line, dotted line, and dotted dotted line are for the original spectra and the fourth-, fifth-, and sixth-order polynomial fitted spectra, respectively.

stabilized 785 nm diode laser, a transmissive imaging spectrograph (HoloSpec-*f*/2.2, Kaiser, Ann Arbor, MI) with a volume phase holographic grating (HSG-785-LF, Kaiser), an NIR optimized charge-coupled device (CCD) detector (LN/CCD-EEV 1024 × 256, Princeton Instruments, Trenton, NJ), and a specially designed Raman probe. The 785 nm laser is coupled to a 200 μm core diameter fiber and delivered to skin at a spot 3.5 mm in diameter. The Raman signal is collected by the Raman probe and delivered to the spectrograph by a fiber bundle (58 × 100 μm core diameter fiber, NA = 0.22). The backscattering of the laser beam is rejected by a high-grade 785 nm long pass filter (Semrock, Rochester, NY). The laser intensity is well below the ANSI standard for skin, and the patients wear a pair of protective eyeglasses during the measurement. For *in vivo* measurements, ethics approval was obtained from the Clinical Research Ethics Board at the University of British Columbia and informed consent was obtained prior to human volunteer measurement. Three sets of spectra are chosen to represent three different situations of

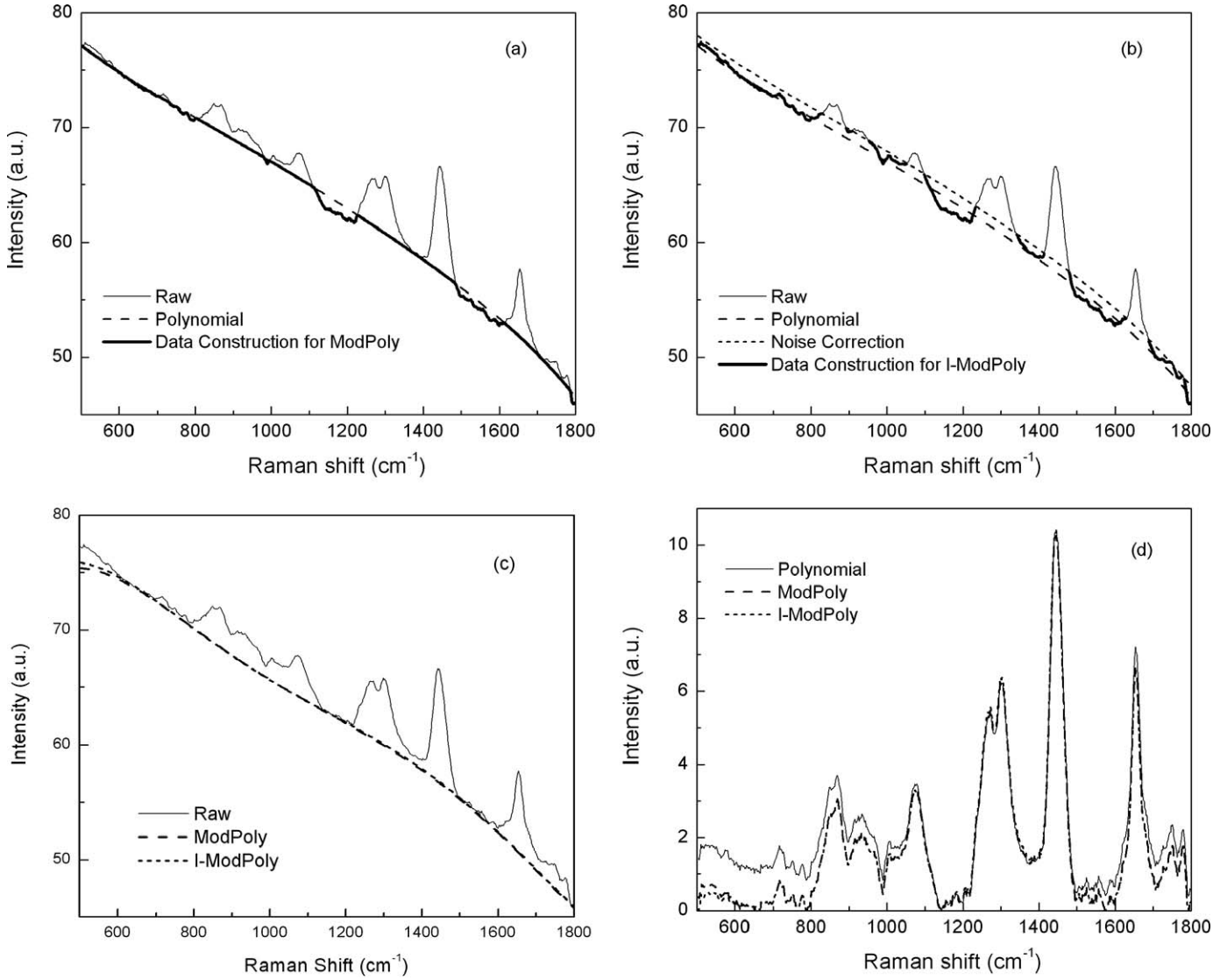

FIG. 4. Fluorescence background removal of high SNR measurement from a volunteer's extensor forearm skin. (**a**) Data construction for the ModPoly method, (**b**) data construction for the I-ModPoly method, (**c**) final fitted fluorescence background, and (**d**) final pure Raman spectra fitted using the three different polynomial methods.

spectra with high signal-to-noise ratio (SNR), low SNR, and intense Raman peaks.

Figure 4 shows the fluorescence background removals for a high SNR spectrum from a volunteer's extensor forearm skin, using the fifth-order single polynomial, the fifth-order ModPoly, and the fifth-order I-ModPoly methods. Figures 4a and 4b show the data construction for the second iteration input for the ModPoly fitting and the I-ModPoly method, respectively. Note that in the I-ModPoly method, the data construction is not based on the fitting function as in ModPoly, but rather on the fitting function shifted upward by the amount of *DEV*. The major peak regions are also removed for the next rounds of fitting. The final fitted fluorescence background and the final pure Raman spectra derived from the three different polynomial methods are shown in Figs. 4c and 4d, respectively. For high SNR spectra, ModPoly and I-ModPoly methods are much better than a single polynomial fitting. They produce almost identical fluorescence backgrounds and Raman spectra, but the time cost for the I-ModPoly fitting method is 16 times less than the ModPoly fitting method for this case. A number of Raman peaks were obtained for human skin, such as the most intense Raman peak at 1445 cm^{-1} assigned to the CH_2 deformations of proteins and lipids; and the second strongest Raman peak at 1655 cm^{-1} assigned to protein vibrational modes involving the C=O stretching mode of amide I bonds, which largely originates from collagen and elastin in dermis. The Raman peak at 1267 cm^{-1} is assigned to CN stretching and NH bending mode of amide III. The peak assignment is consistent with the peak ratio analysis of normal human skin.[21]

Figure 5 shows the fluorescence background removal of a set of low SNR spectra from a volunteer's facial cheek skin, which typically exhibits high autofluorescence. The fifth-order polynomial was used for the three methods. Figures 5a and 5b show the data construction of the ModPoly and the I-ModPoly fitting methods, respectively. For illustration purpose, only the spectra within the range 600–1200 cm^{-1} are plotted. Note that the noise is incorrectly regarded as signal and is replaced by the fitting function in the ModPoly method,

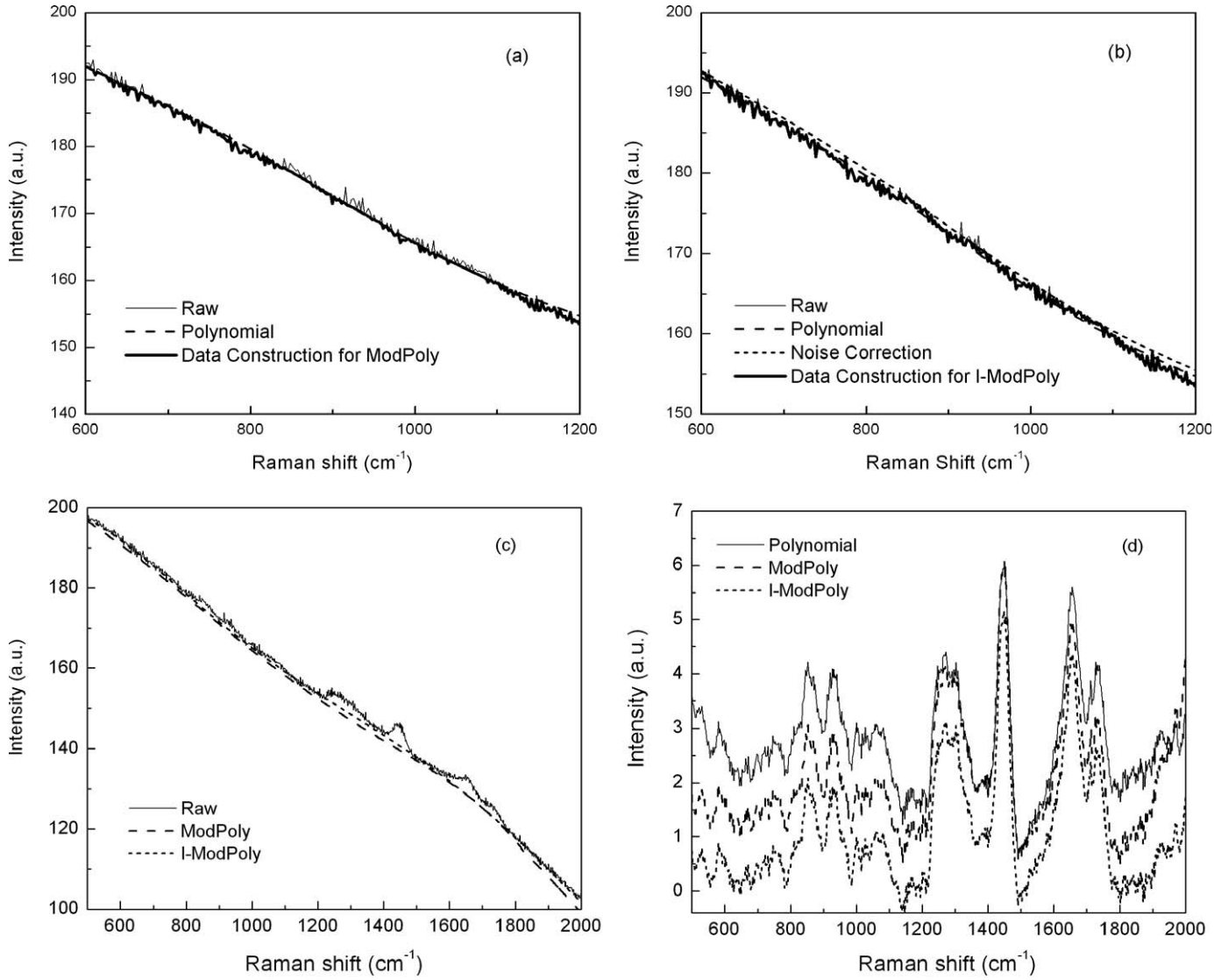

FIG. 5. Fluorescence background removal of low SNR spectra from a volunteer's facial cheek skin. (**a**) Data construction for the ModPoly method, (**b**) data construction for the I-ModPoly method, (**c**) final fitted fluorescence background, and (**d**) final pure Raman spectra fitted using the three different polynomial methods (after a five-point boxcar smoothing). To better demonstrate the noise effect, (a) and (b) show only a portion of the entire spectrum.

whereas noise is untouched in the I-ModPoly method. The final fitted fluorescence background and the final pure Raman spectra fitted for the three different polynomial methods are shown in Figs. 5c and 5d, respectively. It is clearly apparent that single polynomial fitting is less efficient for removing the fluorescence background. ModPoly and I-ModPoly substantially improve the fitting process. However, for the I-ModPoly method the final fluorescence spectra are shifted upward by an amount equivalent to the noise level for the ModPoly method. I-ModPoly fitting produces more realistic pure Raman spectra and takes 70 times less computing time than the ModPoly method.

Figure 6 shows the fluorescence background removal for solid phase urocanic acid (Sigma Aldrich), which exhibits multiple intense Raman peaks. Figure 6a shows the raw spectra and the fluorescence background, and Fig. 6b shows the final pure Raman spectra fitted by the three different methods with the fifth-order polynomial fitting. The single polynomial fitting method does a somewhat poor job of removing the background in the setting of multiple distinct and intense Raman peaks. The intense peak at 1664 cm^{-1} heavily biases the single polynomial fitting. Even the ModPoly fitting cannot fully correct the bias of the major peaks. However, for the I-ModPoly method, because the peak regions are removed in the fitting, the bias of the major peaks is minimized. Potential artifact peaks at both the upper and lower spectral boundary regions are also prevented. In this case, the computing time is 50 times less than the ModPoly method.

Figure 7 shows the pure Raman spectra of the solid phase urocanic acid sample after the fluorescence background removal using the above three methods with the choice of the fourth- (solid line), fifth- (dashed line), and sixth-order (dotted line) polynomial fitting. No method was found totally immune to the choice of polynomial order. Raman spectra from the single polynomial fitting differ significantly for the choice of different orders. ModPoly reduces the difference between the choices of different orders, and the I-ModPoly is the least dependent on the choice of polynomial order.

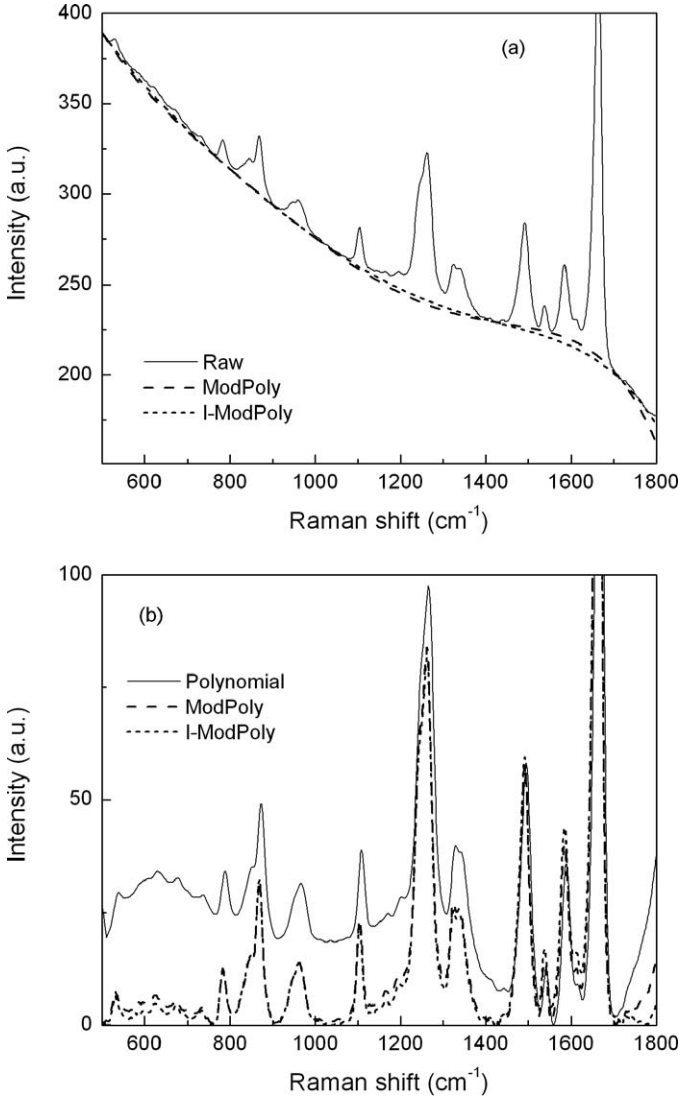

FIG. 6. Fluorescence background removal of spectra with intense Raman peaks. (**a**) Final fluorescence background, (**b**) final pure Raman spectra fitted using the three different polynomial methods. An intense Raman peak at 1664 cm^{-1} substantially influences the polynomial fitting and ModPoly fitting, but this bias is minimal with the I-ModPoly fitting method.

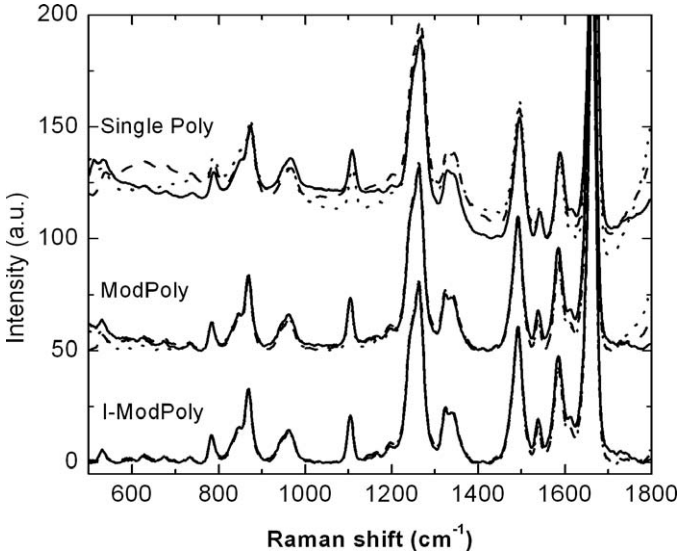

FIG. 7. Pure Raman spectra of solid phase urocanic acid obtained from the three methods with the choice of the fourth-, fifth-, and sixth-order polynomial fitting. Fourth- to sixth-order polynomial fitting is the most used method for fluorescence background removal in tissue Raman measurement. Note that the spectra from single polynomial fitting are heavily dependent on the choice of polynomial order. ModPoly fitting improves the independence from the polynomial orders, and I-ModPoly is almost immune to the choice of polynomial orders.

CONCLUSION

In conclusion, we propose a method for improving fluorescence background removal using modified multi-polynomial fitting by combining the modified multi-polynomial fitting with a peak-removal procedure and incorporating a statistical approach to reducing the effects of noise. This algorithm takes into account the effects of noise level and peak contribution, thereby suppressing the undesirable artificial peaks that may occur in polynomial fittings. The algorithm also takes less computing time, favored by real-time applications. This method produces almost identical results with the modified multi-polynomial fitting method in high SNR spectra, but significantly improves the fluorescence background removal in low SNR spectra over the modified multi-polynomial fitting method, and noticeable improvements are also demonstrated for spectra with intense Raman peaks. Reproducible and consistent pure Raman spectra that are relatively free of fluorescence contributions can be automatically obtained with no *a priori* knowledge of the Raman peak locations or pretreatment, and it is therefore recommended as a preferred algorithm for real-time biomedical Raman applications.

ACKNOWLEDGMENTS

The authors acknowledge Wei Zhang for his assistance in experiments. This work was supported by the National Cancer Institute of Canada with funds from the Canadian Cancer Society, the Canadian Institutes of Health Research, the Canadian Dermatology Foundation, and the BC Hydro Employees' Community Services Fund.

1. R. Richards-Kortum and E. Sevick-Muraca, Annu. Rev. Phys. Chem. **47,** 555 (1996).
2. A. Mahadevan-Jansen and R. Richards-Kortum, J. Biomed. Opt. **1,** 31 (1996).
3. E. B. Hanlon, R. Manoharan, T. W. Koo, K. E. Shafer, J. T. Motz, M. Fitzmaurice, J. R. Kramer, I. Itzkan, R. R. Dasari, and M. S. Feld, Phys. Med. Biol. **45,** R1 (2000).
4. M. G. Shim and B. C. Wilson, J. Raman Spectrosc. **28,** 131 (1997).
5. Z. Huang, A. McWilliams, H. Lui, D. I. McLean, S. Lam, and H. Zeng, Int. J. Cancer **107,** 1047 (2003).
6. Z. Huang, H. Lui, X. K. Chen, A. Alajlan, D. I. McLean, and H. Zeng, J. Biomed. Opt. **9,** 1198 (2004).
7. Z. Huang, H. Zeng, I. Hamzavi, D. I. McLean, and H. Lui, Opt. Lett. **26,** 1782 (2001).
8. J. T. Motz, S. J. Gandhi, O. R. Scepanovic, A. S. Haka, J. R. Kramer, R. R. Dasari, and M. S. Feld, J. Biomed. Opt. **10,** 031113 (2005).
9. G. Schulze, A. Jirasek, M. L. Yu, A. Lim, R. F. B. Turner, and M. W. Blades, Appl. Spectrosc. **59,** 545 (2005).
10. C. A. Lieber and A. Mahadevan-Jansen, Appl. Spectrosc. **57,** 1363 (2003).
11. P. Shreve, N. J. Cherepy, and R. A. Mathies, Appl. Spectrosc. **46,** 707 (1992).
12. J. J. Baraga, M. S. Feld, and R. P. Rava, Appl. Spectrosc. **46,** 187 (1992).
13. M. D. Morris, P. Matousek, M. Towrie, A. W. Parker, A. E. Goodship, and E. R. Draper, J. Biomed. Opt. **10,** 14014 (2005).
14. A. K. Atakan, W. E. Blass, and D. E. Jennings, Appl. Spectrosc. **34,** 369 (1980).
15. P. A. Mosier-Boss, S. H. Lieberman, and R. Newbery, Appl. Spectrosc. **49,** 630 (1995).

16. S. E. Bell, E. S. O. Bourguignon, and A. Dennis, Analyst (Cambridge, U.K.) **123,** 1729 (1998).
17. P. Matousek, M. Towrie, and A. W. Parker, Appl. Spectrosc. **59,** 848 (2005).
18. J. F. Brennan, Y. Wang, R. R. Dasari, and M. S. Feld, Appl. Spectrosc. **51,** 201 (1997).
19. A. Mahadevan-Jansen, M. F. Mitchell, N. Ramanujam, U. Utzinger, and R. Richards-Kortum, Photochem. Phobiol. **68,** 427 (1998).
20. H. G. M. Edwards, A. C. Williams, and B. W. Barry, J. Mol. Struct. **347,** 379 (1995).
21. Z. Huang, H. Zeng, I. Hamzavi, D. I. McLean, and H. Lui, Proc. SPIE-Int. Soc. Opt. Eng. **4597,** 109 (2001).
22. H. P. Bschman, E. T. Marple, M. L. Wash, B. Bennett, T. C. Schut, M. Brochert, H. A. Bruining, A. V. Bruschke, A. van der Laarse, and G. J. Puppels, Anal. Chem. **72,** 3771 (2000).
23. P. J. Caspers, G. W. Lucassen, R. Wolthuis, H. A. Bruining, and G. J. Puppels, Biospectroscopy **4,** S31 (1998).
24. P. J. Caspers, G. W. Lucassen, and G. J. Puppels, Biophys. J. **85,** 572 (2003).
25. L. Chrit, C. Hadjur, S. Morel, G. Sockalingum, G. Lebourdon, F. Leroy, and M. Manfait, J. Biomed. Opt. **10,** 44007 (2005).
26. A. M. K. Enejder, T. G. Scecina, J. Oh, M. Hunter, W. Shih, S. Sasic, G. L. Horowitz, and M. S. Feld, J. Biomed. Opt. **10,** 031114 (2005).
27. J. L. Lambert, C. C. Pelletier, and M. Brochert, J. Biomed. Opt. **10,** 031110 (2005).
28. J. T. Motz, M. Fitzmaurice, A. Miller, S. J. Gandhi, A. S. Haka, L. H. Galindo, R. R Dasari, J. R. Kramer, and M. S. Feld, J. Biomed. Opt. **11,** 021003 (2006).